

IDENTIFICATION OF THE SOURCE REGION OF A “HALO” CORONAL MASS EJECTION USING METER-WAVELENGTH RADIO DATA

C. KATHIRAVAN¹ AND R. RAMESH²

Received 2005 March 8; accepted 2005 May 16; published 2005 June 17

ABSTRACT

We present meter-wavelength observations of the solar corona close to the onset of the “halo” coronal mass ejection (CME) of 1998 January 21 and estimate the change in electron density with time through a reproduction of the observed two-dimensional radio brightness distribution using a ray-tracing technique. Our calculations show that the average density above the background in the southeast quadrant of the corona overlying the visible solar disk had increased significantly (from 0 to 18), in the aftermath of the CME liftoff. This indicates that the source region of the event must have been located at a lower level of the solar atmosphere in that area. The rate of mass injection corresponding to the above change in density was found to be $\approx 8.8 \times 10^{15} \text{ g hr}^{-1}$.

Subject headings: solar-terrestrial relations — Sun: activity — Sun: corona — Sun: radio radiation

1. INTRODUCTION

The observations with conventional “white-light” coronagraphs are the historical and empirical foundations of our present knowledge of coronal mass ejections (CMEs). But by their very nature, the coronagraphs have an occulting disk to block the direct photospheric light, and hence the source region of a CME cannot be observed using them. The situation is severe, particularly for CMEs directed along the Sun-Earth axis, termed “halo” CMEs by Howard et al. (1982), since they originate close to the center of the visible hemisphere of the solar disk. Attempts have been made to identify the location of eruption using soft X-ray (Hudson & Webb 1997; Plunkett et al. 1997), EUV (Thompson et al. 1998; Plunkett et al. 1998; Zhukov & Auchère 2004), and microwave (Filippov 1998; Dougherty et al. 2002; Gopalswamy et al. 2003) data. Radio observations in the meter-wavelength range also play a useful role in this connection, since they do not have the limitation of an occulting disk and a CME can be directly imaged in thermal bremsstrahlung emission from the excess electrons in its frontal loop (Gopalswamy & Kundu 1992; Bastian & Gary 1997; Kathiravan et al. 2002). The sky-plane speed and acceleration of the latter, particularly in the region of the solar atmosphere beneath the occulting disk of a coronagraph, can be estimated in a straightforward manner (Ramesh et al. 2003). Again, one can observe activity at any longitude, similar to X-ray and EUV wavelengths (Ramesh & Sastry 2000; Ramesh 2000). The “true” speed of a CME in three-dimensional space can also be determined through ray-tracing analysis of the observed radio brightness distribution (Kathiravan & Ramesh 2004). In this Letter, we report on our attempt to obtain quantitative information on the source region of a halo CME in an independent manner through ray-tracing analysis of the meter-wavelength radioheliogram close to its onset.

2. OBSERVATIONS

The radio data reported were obtained on 1998 January 21 at 109 MHz with the Gauribidanur radioheliograph (GRH; Ramesh et al. 1998), operating near Bangalore in India. The characteristics of the array at the above frequency are the minimum detectable flux limit $\approx 0.02 \text{ sfu}$ ($1 \text{ sfu} = 10^{-22} \text{ W m}^{-2} \text{ Hz}^{-1}$),

angular resolution $\approx 7' \times 11'$ (R.A. \times decl.), and the field of view $\approx 3^\circ \times 5^\circ$ (R.A. \times decl.). The calibration scheme used for processing of the GRH data makes use of the redundancy in the length and orientation of the various baseline vectors and enables us to image the solar corona with a dynamic range of $\geq 20 \text{ dB}$ (Ramesh 1998; Ramesh et al. 1999). This is useful in detecting thermal emission from weak density enhancement associated with coronal streamers, CMEs, etc., in a better manner. According to the CME catalog³ for the year 1998, a full halo event was observed on 1998 January 21 by the Large Angle and Spectroscopic Coronagraph (LASCO; Brueckner et al. 1995) on board the *Solar and Heliospheric Observatory (SOHO)*; Fleck et al. 1995). The event was first observed above the southern quadrant of the occulting disk of the LASCO C2 coronagraph around 06:37:25 UT. Its leading edge was located at a radial distance of about $2.75 R_\odot$ ($R_\odot = \text{solar radius} = 6.96 \times 10^5 \text{ km}$) at that time. The extrapolated onset time of the event is 05:09:09 UT. The speed along the line of sight and in the plane of the sky are ≈ 318 and 485 km s^{-1} , respectively (Kathiravan & Ramesh 2004). The CME was associated with a H α filament eruption from the location (S57°, E19°)⁴ on the solar disk between 04:00 and 06:03 UT on that day (Gopalswamy et al. 2000; Zhou et al. 2003). Figures 1 and 2 show the radioheliogram obtained with the GRH on 1998 January 21 at 05:01 and 6:01 UT, before and after the onset of the CME, respectively. There is noticeable enhanced emission in the radioheliogram obtained at 06:01 UT in the aftermath of the CME liftoff.

3. ANALYSIS AND RESULTS

The ray-tracing technique described in our earlier papers (Ramesh & Sastry 2000; Kathiravan et al. 2002; Kathiravan & Ramesh 2004) is used to reproduce the observed radioheliogram. Figures 3 and 4 show the brightness distribution obtained through ray-tracing calculations for the radioheliogram observed before (Fig. 1) and after (Fig. 2) the eruption of the CME, respectively. There is a good similarity between the corresponding images. The assumed values for the electron temperature and density of the “background” solar corona are $\approx 1.0 \times 10^6 \text{ K}$ and $0.45 \times \text{Newkirk density}$ (Newkirk 1961), respectively, for both the events. Note that according to the $1 \times \text{Newkirk density}$ model,

¹ Indian Institute of Astrophysics, Bangalore 560 034, India; kathir@iiap.res.in.

² Centre for Research and Education in Science and Technology, Indian Institute of Astrophysics, Hosakote 562 114, India; ramesh@iiap.res.in.

³ See http://cdaw.gsfc.nasa.gov/CME_list.

⁴ Solar-Geophysical Data, 647, Part II, 1998 July.

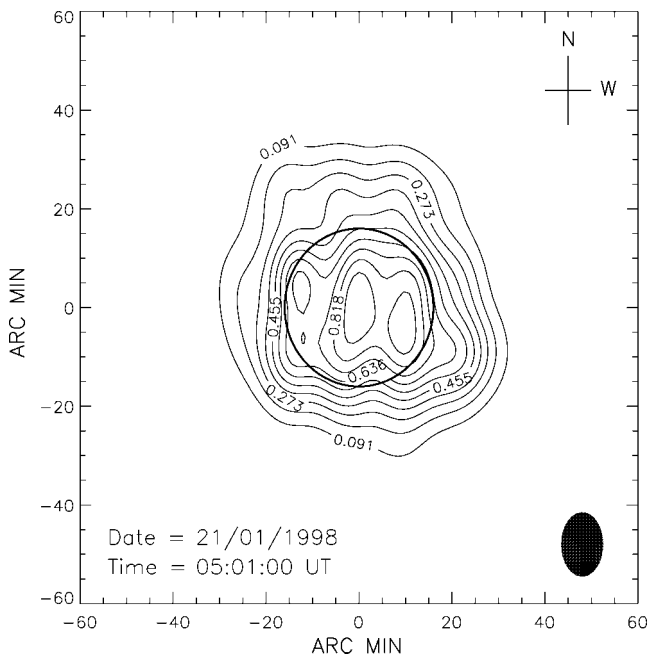


FIG. 1.—Radioheliogram obtained with the GRH at 109 MHz on 1998 January 21 at 05:01 UT. The peak brightness temperature is $\sim 2.10 \times 10^6$ K, and the contour interval is 2.1×10^5 K. The open circle at the center represents the solar limb. The filled contour near the bottom right corner represents the instrument beam at the observing frequency.

the 109 MHz plasma level in the background corona will be located at a radial distance of $\approx 1.22 R_\odot$ (from the center of the Sun). But in order to obtain a better reproduction of the observed radioheliogram in Figures 1 and 2, we used the $0.45 \times$ Newkirk density model. The 109 MHz plasma level in the latter is located at a radial distance of $\approx 1.11 R_\odot$. The parameters of the different discrete sources used to obtain Figures 3 and 4 are listed in Tables 1 and 2, respectively. Note that about 15 discrete sources have been used to reproduce the observed brightness distribution in Figures 1 and 2. Since the source region of 90% of the halo

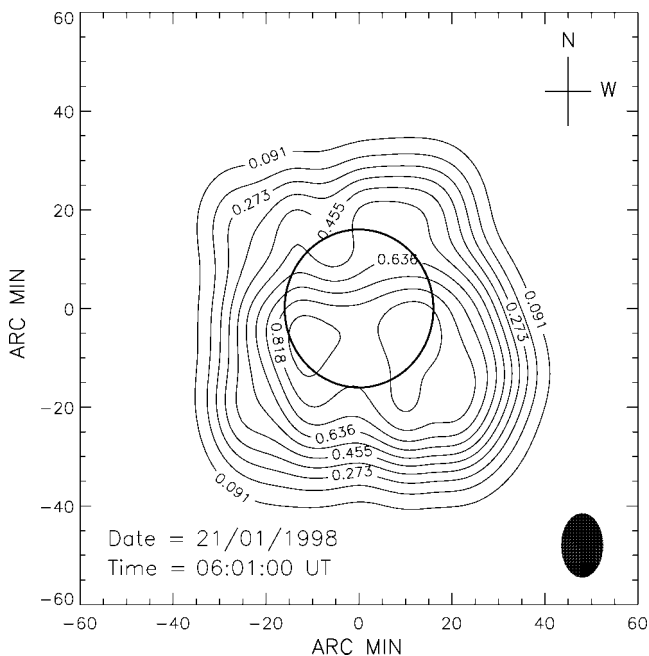


FIG. 2.—Same as Fig. 1, but obtained at 06:01 UT. The peak brightness temperature is $\sim 2.20 \times 10^6$ K, and the contour interval is 2.2×10^5 K.

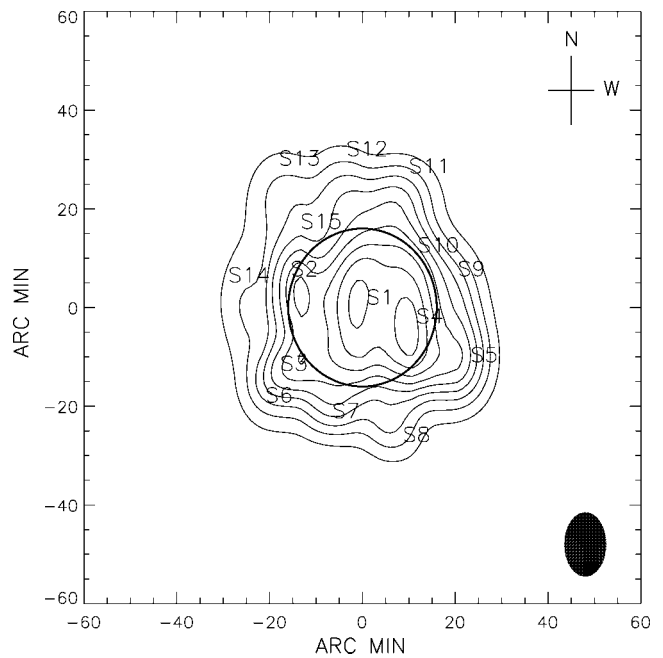


FIG. 3.—Reproduction of radioheliogram in Fig. 1 through ray-tracing technique. The numbers S1–S15 indicate the location of the centroid of the discrete sources used in our calculations. Their parameters are listed in Table 1.

CMEs are located within $\pm 60^\circ$ longitude and latitude on the Sun (Lara et al. 2000), we adopted the following criteria to identify the relevant sources from the above list: (1) the magnitude of the z -coordinate⁵ of the source should be less than $1.0 R_\odot$ and (2) the y -coordinate should be less than $(1 - z^2)^{1/2}$. The sources that meet the above criteria are listed in Table 3. Their longitude and latitude were obtained using the following expressions: $\text{long} = \tan^{-1}(y/x)$ and $\text{lat} = 90^\circ - \cos^{-1}(z/r)$.

⁵ The x -, y -, and z -coordinates in our calculations represent the Earthward, longitudinal, and latitudinal directions on the Sun; they are in units of solar radius.

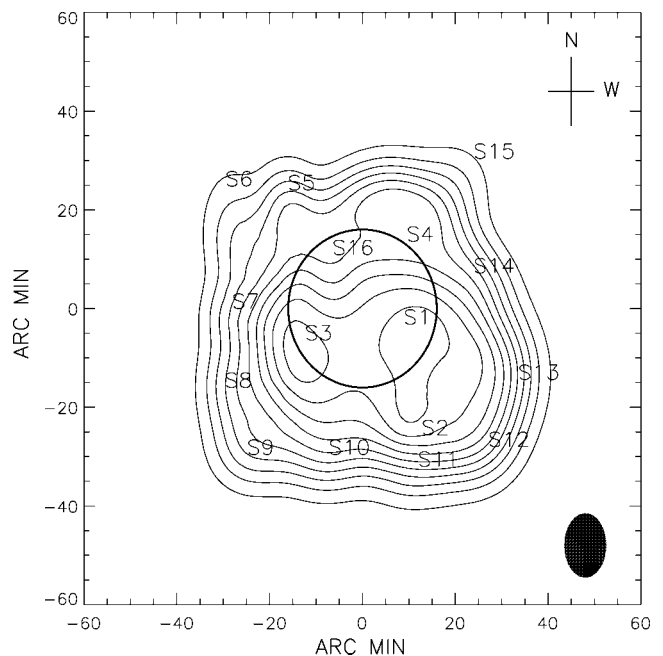


FIG. 4.—Same as Fig. 3, but for the radioheliogram in Fig. 2. The parameters of the sources S1–S16 are listed in Table 2.

TABLE 1
PARAMETERS OF THE DISCRETE SOURCES IN FIGURE 3

| Source | Position ^a (x_n, y_n, z_n) | Size ^b [(σ_x) _n , (σ_y) _n , (σ_z) _n] | Density Factor ^c (C_n) |
|--------|--|---|--|
| S1 | 1.50, 0.06, 0.04 | 0.22, 0.29, 0.50 | 16.0 |
| S2 | 2.30, -0.96, 0.40 | 0.22, 0.16, 0.55 | 23.0 |
| S3 | 1.30, -1.10, -0.80 | 0.22, 0.32, 0.19 | 3.0 |
| S4 | 1.85, 0.73, -0.20 | 0.22, 0.26, 0.55 | 30.0 |
| S5 | 1.50, 1.46, -0.69 | 0.22, 0.32, 0.47 | 10.6 |
| S6 | 1.30, -1.30, -1.20 | 0.22, 0.28, 0.35 | 4.0 |
| S7 | 1.60, -0.40, -1.40 | 0.22, 0.22, 0.22 | 5.0 |
| S8 | 1.30, 0.55, -1.70 | 0.22, 0.22, 0.22 | 5.0 |
| S9 | 1.50, 1.29, 0.40 | 0.22, 0.33, 0.39 | 5.0 |
| S10 | 1.60, 0.75, 0.70 | 0.22, 0.26, 0.22 | 10.0 |
| S11 | 1.30, 0.63, 1.70 | 0.22, 0.40, 0.33 | 6.5 |
| S12 | 1.30, -0.21, 1.92 | 0.22, 0.17, 0.33 | 5.4 |
| S13 | 1.30, -1.12, 1.80 | 0.22, 0.40, 0.51 | 7.0 |
| S14 | 1.30, -1.80, 0.32 | 0.22, 0.32, 0.67 | 2.1 |
| S15 | 1.26, -0.83, 1.00 | 0.22, 0.45, 0.35 | -0.4 |

^a The coordinates of the source centroid in units of solar radius.
^b Size of the sources along x -, y -, and z -axes, in units of solar radius.
^c The negative value of S15 indicates a reduction in density with respect to the background.

Here $r = (x^2 + y^2 + z^2)^{1/2}$ is the radial distance of the source from the center of the Sun. The error involved in the longitude and latitude estimation is $\approx \pm 15^\circ$. We calculated the change in density enhancement ($\Gamma = \Delta C_n / \Delta t$, where C_n is the density factor) of the radio sources in the corona overlying the visible solar disk between 05:01 and 06:01 UT, and the average values in the different quadrants are $\Gamma_{NE} = 0$, $\Gamma_{SE} = 18$, $\Gamma_{SW} = 4$, and $\Gamma_{NW} = 2 \text{ hr}^{-1}$ (Fig. 5). There is a significant increase in density in the southeast quadrant. This indicates that the source region of the CME must have been located in that area, below the altitude from where the observed 109 MHz radiation has originated. The enhanced emission is due to thermal bremsstrahlung from the excess electrons associated with the CME. It is interesting to note that the $H\alpha$ filament eruption that was temporally associated with the CME in the present case was also from the same quadrant, i.e., S57 E19. An inspection of Table 3 indicates that the change in density in the southeast quadrant is mainly due to the discrete source S4 used in the ray-tracing calculations to reproduce the observed radioheliogram at 06:01 UT. We calculated its mass using the relation $M = N_e V$, where N_e and V are the density and volume ($\sigma_x \times \sigma_y \times \sigma_z$) of the structure (see

TABLE 2
PARAMETERS OF THE DISCRETE SOURCES IN FIGURE 4

| Source | Position ^a (x_n, y_n, z_n) | Size ^b [(σ_x) _n , (σ_y) _n , (σ_z) _n] | Density Factor ^c (C_n) |
|--------|--|---|--|
| S1 | 1.72, 0.56, -0.20 | 0.32, 0.74, 0.59 | 34.0 |
| S2 | 1.60, 0.80, -1.60 | 0.32, 0.47, 0.52 | 16.0 |
| S3 | 1.70, -0.77, -0.40 | 0.22, 0.55, 0.71 | 18.0 |
| S4 | 1.10, 0.60, 0.85 | 0.22, 0.63, 0.77 | 18.0 |
| S5 | 1.00, -1.00, 1.50 | 0.22, 0.22, 0.50 | 8.0 |
| S6 | 0.60, -1.84, 1.55 | 0.22, 0.32, 0.77 | 7.0 |
| S7 | 1.10, -1.75, 0.00 | 0.22, 0.32, 0.32 | 7.5 |
| S8 | 0.80, -1.85, -1.00 | 0.22, 0.32, 0.45 | 9.0 |
| S9 | 1.20, -1.55, -1.85 | 0.22, 0.45, 0.45 | 17.3 |
| S10 | 1.30, -0.45, -1.85 | 0.22, 0.39, 0.52 | 12.4 |
| S11 | 1.00, 0.75, -2.00 | 0.22, 0.45, 0.55 | 10.0 |
| S12 | 1.00, 1.70, -1.75 | 0.22, 0.45, 0.50 | 22.0 |
| S13 | 1.40, 2.10, -0.90 | 0.22, 0.45, 0.67 | 22.0 |
| S14 | 1.10, 1.50, 0.45 | 0.22, 0.45, 0.32 | 10.0 |
| S15 | 0.40, 1.50, 1.90 | 0.22, 0.39, 0.45 | 7.0 |
| S16 | 1.70, -0.40, 0.68 | 0.22, 0.19, 0.39 | -0.3 |

^a The coordinates of the source centroid in units of solar radius.
^b Size of the sources along x -, y -, and z -axes, in units of solar radius.
^c The negative value of S16 indicates a reduction in density with respect to the background.

TABLE 3
THE LONGITUDE AND LATITUDE OF THE CORONAL RADIO SOURCES ABOVE THE VISIBLE SOLAR DISK

| Event Time (UT) | Source | Longitude (deg) | Latitude (deg) | Density Factor (C_n) |
|-----------------|--------|-----------------|----------------|--------------------------|
| 05:01 | S1 | 2W | 2N | 16.0 |
| | S4 | 20W | 5S | 30.0 |
| 06:01 | S1 | 18W | 6S | 34.0 |
| | S3 | 24E | 12S | 18.0 |
| | S4 | 29W | 34N | 18.0 |
| | S16 | 13E | 21N | -0.3 |

Table 2), and the value is $\approx 8.8 \times 10^{15} \text{ g}$. Note that no density enhancement was observed above the visible solar disk in the southeast quadrant prior to the CME liftoff (see Table 3). Therefore, the above mass must have been injected into the upper layers of the solar atmosphere in a period of $\leq 1 \text{ hr}$, during the propagation of the CME. Our estimate is in good agreement with the mass loss reported in association with the launch of a CME (Hudson et al. 1996; Sterling & Hudson 1997; Gopalswamy & Hanaoka 1998; Ramesh & Sastry 2000).

In conclusion, our results indicate that ground-based low-frequency (30–110 MHz) radio observations can be a useful

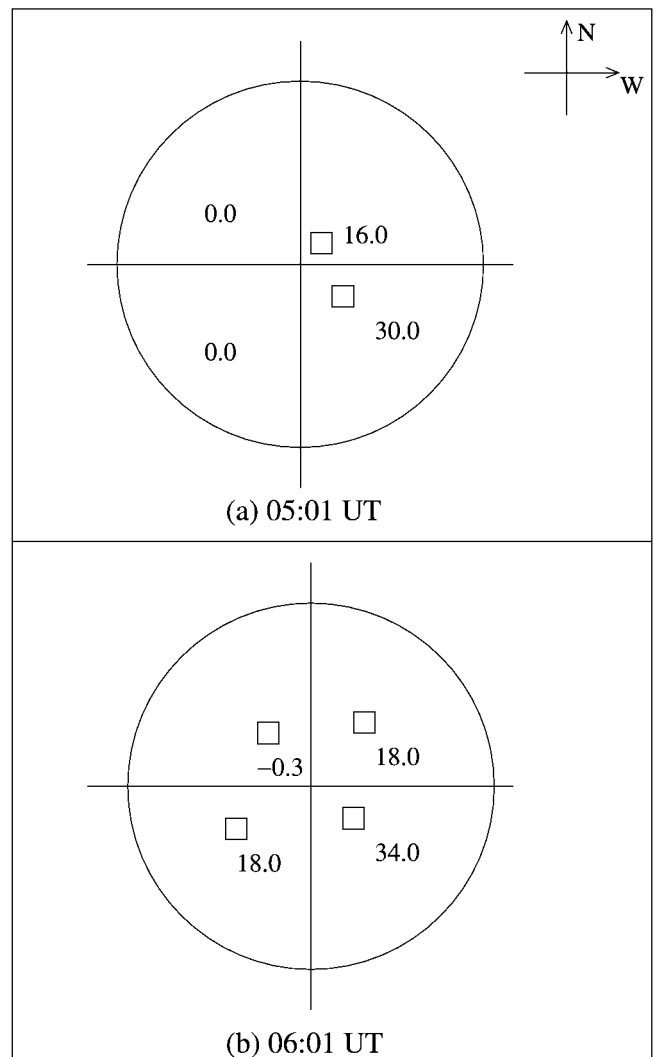


FIG. 5.—Graphical illustration of the quadrant-wise average density enhancement/depletion in our ray-tracing calculations. The open circles in (a) and (b) represent the solar disk. A comparison of the two panels indicates a significant increase in density in the southeast quadrant.

and independent tool to identify the source region of a CME on the solar disk, since the corona overlying the visible solar disk can be imaged without any limitation. Again, the optical depth of the emission from the background corona in the above frequency range is not very large. Thus, the radio counterpart of a CME can be observed close to its onset with a better contrast (Ramesh 2005).

We thank the staff of Gauribidanur radio observatory for their help in data collection and maintenance of the antenna

and receiver systems. We also thank the referee for comments that helped us to present the results more clearly. The *SOHO* data are produced by a consortium of the Naval research laboratory (US), Max-Planck-Institut für Aeronomie (Germany), Laboratoire d'Astronomie (France), and the University of Birmingham (UK). *SOHO* is a project of international cooperation between the ESA and NASA. The CME catalog is generated and maintained by the Center for Solar Physics and Space Weather at the Catholic University of America in cooperation with the Naval Research Laboratory and NASA.

REFERENCES

- Bastian, T. S., & Gary, D. E. 1997, *J. Geophys. Res.*, 102, 14031
 Brueckner, G. E., et al. 1995, *Sol. Phys.*, 162, 357
 Dougherty, B. L., et al. 2002, *ApJ*, 577, 457
 Filippov, B. P. 1998, in *ASP Conf. Ser. 150, New Perspectives on Solar Prominences*, ed. D. Rust, D. F. Webb, & B. Schmieder (IAU Colloq. 167; San Francisco: ASP), 342
 Fleck, B., Domingo, V., & Poland, A., ed. 1995, *The SOHO Mission* (Dordrecht: Kluwer)
 Gopalswamy, N., & Hanaoka, Y. 1998, *ApJ*, 498, L179
 Gopalswamy, N., & Kundu, M. R. 1992, *ApJ*, 390, L37
 Gopalswamy, N., et al. 2000, *J. Geophys. Res.*, 27, 1427
 ———. 2003, *ApJ*, 586, 562
 Hudson, H. S., Acton, L. W., & Freeland, S. L. 1996, *ApJ*, 470, 629
 Hudson, H. S., & Webb, D. F. 1997, *Geophys. Monogr.*, 99, 27
 Howard, R. A., et al. 1982, *ApJ*, 263, L101
 Kathiravan, C., & Ramesh, R. 2004, *ApJ*, 610, 532
 Kathiravan, C., Ramesh, R., & Subramanian, K. R. 2002, *ApJ*, 567, L93
 Lara, A., Gopalswamy, N., DeForest, C. 2000, *J. Geophys. Res.*, 27, 1435
 Newkirk, G. A., Jr. 1961, *ApJ*, 133, 983
 Plunkett, S. P., et al. 1997, *Sol. Phys.*, 175, 699
 ———. 1998, *Geophys. Res. Lett.*, 25, 2477
 Ramesh, R. 1998, Ph.D thesis, Bangalore Univ.
 ———. 2000, *Sol. Phys.*, 196, 213
 ———. 2005, in *IAU Symp. 226, Coronal and Stellar Mass Ejections*, ed. K. P. Dere, J. Wang, & Y. Yan (Dordrecht: Kluwer), 83
 Ramesh, R., Kathiravan, C., & Sastry, Ch. V. 2003, *ApJ*, 591, L163
 Ramesh, R., & Sastry, Ch. V. 2000, *A&A*, 358, 749
 Ramesh, R., Subramanian, K. R., & Sastry, Ch. V. 1999, *A&AS*, 139, 179
 Ramesh, R., Subramanian, K. R., SundaraRajan, M. S., & Sastry, Ch. V. 1998, *Sol. Phys.*, 181, 439
 Sterling, A. C., & Hudson, H. S. 1997, *ApJ*, 491, L55
 Thompson, B. J., et al. 1998, *Geophys. Res. Lett.*, 25, 2465
 Zhou, G., Wang, J., & Cao, Z. 2003, *A&A*, 397, 1057
 Zhukov, A. N., & Auchère, F. 2004, *A&A*, 427, 705